IOP Publishing and International Atomic Energy Agency Nuclear Fusion
Nucl. Fusion **51** (2011) 063022 (11pp) doi:10.1088/0029-5515/51/6/063022

L-mode validation studies of gyrokinetic turbulence simulations via multiscale and multifield turbulence measurements on the DIII-D tokamak

T.L. Rhodes[1], C. Holland[2], S.P. Smith[3], A.E. White[4], K.H. Burrell[3], J. Candy[3], J.C. DeBoo[3], E.J. Doyle[1], J.C. Hillesheim[1], J.E. Kinsey[3], G.R. McKee[5], D. Mikkelsen[6], W.A. Peebles[1], C.C. Petty[3], R. Prater[3], S. Parker[7], Y. Chen[7], L. Schmitz[1], G.M. Staebler[3], R.E. Waltz[3], G. Wang[1], Z. Yan[5] and L. Zeng[1]

[1] Physics Department and PSTI, University of California, Los Angeles, CA 90095, USA
[2] University of California-San Diego, 9500 Gilman Dr., La Jolla, CA 92093-0417, USA
[3] General Atomics, PO Box 85608, San Diego, CA 92186-5608, USA
[4] Massachusetts Institute of Technology, 77 Massachusetts Ave., Cambridge, MA 02139, USA
[5] Department of Engineering Physics, University of Wisconsin-Madison, 1500 Engineering Dr., Madison,WI 53706, USA
[6] Princeton Plasma Physics Laboratory, PO Box 451, Princeton, NJ 08543-0451, USA
[7] Center for Integrated Plasma Studies, University of Colorado, 20000 Colorado Ave., Boulder, CO 80309-0390, USA

Received 14 January 2011, accepted for publication 7 April 2011
Published 13 May 2011
Online at stacks.iop.org/NF/51/063022

Abstract
A series of carefully designed experiments on DIII-D have taken advantage of a broad set of turbulence and profile diagnostics to rigorously test gyrokinetic turbulence simulations. In this paper the goals, tools and experiments performed in these validation studies are reviewed and specific examples presented. It is found that predictions of transport and fluctuation levels in the mid-core region ($0.4 < \rho < 0.75$) are in better agreement with experiment than those in the outer region ($\rho \geqslant 0.75$) where edge coupling effects may become increasingly important and multiscale simulations may also be necessary. Validation studies such as these are crucial in developing confidence in a first-principles based predictive capability for ITER.

(Some figures in this article are in colour only in the electronic version)

1. Introduction

First-principles predictive simulation of plasma confinement and performance is one of the over-arching goals of fusion research today [1, 2]. Numerous experiments, measurements and simulation codes from across the world are focused on this goal (see [3–10] for recent work). On the DIII-D tokamak a series of carefully designed experiments have taken advantage of a broad set of turbulence and profile diagnostics to address this 'grand challenge'. In this paper the goals, tools and experiments performed in these validation studies are reviewed and specific examples presented. Although still in the early days, this effort has found that modelling predictions of L-mode transport and fluctuation levels in the mid-core region ($0.4 < \rho < 0.75$) are often in better agreement with experiment than those in the outer region ($\rho \geqslant 0.75$). Here ρ is the radial coordinate defined as the normalized square root of the toroidal magnetic flux. One possible explanation of this discrepancy towards the edge (i.e. the underprediction of turbulence and transport levels) is the increasing importance of edge effects as the plasma boundary is approached (e.g. edge–core coupling [11], avalanches propagating in from the edge [12], etc). In order to address such effects, global non-linear simulations from the core to the edge, and perhaps into the scrape-off layer, would be required. Another possible explanation is the increasing importance of

high-k electron temperature gradient (ETG) type modes as the edge is approached. Fully coupled, low through high-k simulations, perhaps indeed coupled with a global simulation, would be necessary to answer this. Simulations at this level remain for the future. Results such as the ones reported here are noteworthy as they point to significant research paths. In addition, validation studies are crucial in developing confidence in a first-principles based predictive capability for ITER and other, future burning plasma experiments.

Validation studies compare measurements with model predictions in order to assess the underlying physics modelling accuracy of the code [13–15]. A related branch of study is that termed verification which deals with the question of whether a code accurately solves the equations upon which it is based. Verification does not address whether the underlying equations adequately represent the real world. Thus a simulation may be verified as correctly solving the equations contained within it but it may fail validation if it does not adequately predict relevant measurements. This study deals only with validation questions and therefore assumes that the codes have been adequately verified (e.g. see [13–15] and references therein for further discussions relating to these two different endeavors).

The question of what constitutes agreement (or alternatively disagreement) arises early in the process. Agreement is often defined to occur when the predicted values lie within the uncertainties of the measured values. Complexity quickly arises as agreement frequently occurs in one set of parameters while significant disagreement is seen in others (e.g. agreement between measured and predicted electron thermal energy fluxes but disagreement between experiment and simulations for the ion thermal energy flux). Various complex measures or metrics have been proposed that deal with this issue that address multiple parameters, radii and uncertainties [15]. However, these metrics are outside the scope of this paper.

Given that experimental measurements are the foundation of this work, it is extremely useful to obtain multiple measures of the same or similar quantities to cross compare for potential bias and error. For example, on DIII-D two measurements of density and electron temperature are obtained via Thomson scattering, electron cyclotron emission (ECE) and reflectometry. In the case of a diagnostic failure, a second measure is invaluable. In addition, errors and bias are potentially resolvable via multiple measurements and in the case of disagreement the experimentalist is alerted to potential issues. Typical validation experiments involve multiple repeat discharges and/or plasma 'jogs' (small rigid body shifts of the plasma) to both scan the fluctuation diagnostics as well as to obtain multiple measures of the density, temperature, safety factor, etc profiles for statistical analysis. These repeat shots and profiles are used to quantify the profile uncertainty and to provide some insight into uncertainties in the resulting transport calculations. Figure 1 diagrams this comparison process. The process is fairly straightforward and natural; however, it is worth pointing out the red horizontal arrow marked 'profiles, flux surface shape, ...'. This is the necessary experimental input to the simulations, thus the predictions are only as good as these inputs and any uncertainties should be propagated through in order to provide an accurate determination of the validity of the comparison.

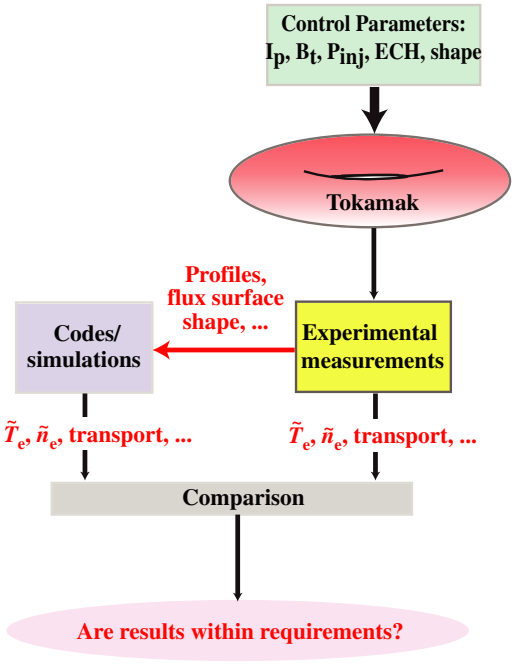

Figure 1. Validation procedure highlighting experimental input to the simulations and comparison of measurements (e.g. $\tilde{T}_e/T_e$, $\tilde{n}_e/n_e$, transport, etc). After the last step an iteration cycle can be commenced by varying one or more of the simulation input parameters (e.g. temperature and density scale lengths, temperatures, flow velocity, etc, re-running the simulation and comparing the new results with experiment.

The input profiles are often the experimentally measured profiles of density, temperatures, etc which the non-linear turbulence simulation codes use to calculate fluctuation levels, transport, etc. An alternate approach is based upon the use of transport models (e.g. TGYRO [16], TRINITY [17], etc) that can use the heating and particle fluxes as inputs (the fluxes themselves are based upon experimental profiles). Based upon assumed turbulent and neoclassical transport models, the transport model then calculates density and temperature profiles that best reproduce the input flux profiles. If the codes are coupled to non-linear simulations then the direct outputs are the sought after fluctuation levels, correlation lengths, etc. Alternatively, the calculated density and temperature profiles can be used as input into non-linear simulations such as GYRO [18, 19], GEM [20], GENE [21], etc.

First-principles based simulations predict transport levels due to simulated turbulence induced transport. For this reason, validation studies compare fundamental level fluctuation parameters (crossphases, correlation lengths, etc), higher level quantities such as amplitudes and power spectra, and finally transport quantities (e.g. thermal and particle fluxes) (see [13] for a discussion of different levels or hierarchies of measurements). Comparisons of thermal and particle fluxes require that the simulated fluxes include the same components included in the experimental fluxes (e.g. convected and conducted terms). Arguably greater care must be taken to accurately compare turbulence measurements with simulation values. Fluctuation measurements have specific wavenumber, frequency and spatial ranges and resolutions that must be

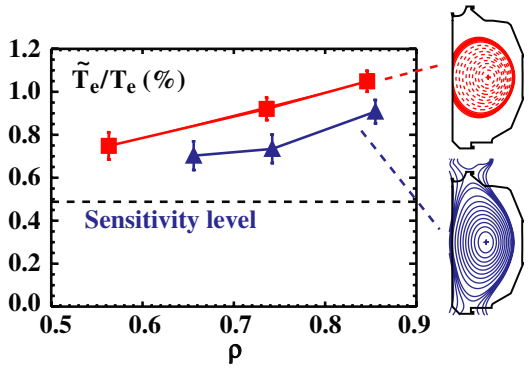

Figure 2. Variation in $\tilde{T}_e/T_e$ measured by CECE with radial position and plasma elongation.

accurately represented when comparing with simulation data. For example, it is insufficient to extract electron temperature fluctuations from a non-linear simulation and compare it directly with a correlation ECE (CECE) measurement of $\tilde{T}_e$. The simulation data must be analysed in a manner analogous to the measurement technique, taking into account wavenumber, time and spatial resolutions, as well as any particular measurement nuances such as cross correlation of multiple spatial volumes (as is done with CECE $\tilde{T}_e$). The codes used in this type of analysis are termed synthetic diagnostics. Specific examples and full descriptions of synthetic diagnostics used at DIII-D can be found in [23–25].

In the next section, the approach used by validation studies at DIII-D is described followed by an overview of the experimental and simulation tools utilized and validation experiments performed at DIII-D. A detailed examination of a recent T_e/T_i scan L-mode experiment is then provided along with linear and non-linear calculations and comparisons followed by a summary and conclusions.

2. Approach to validation studies

The approach to validation studies used at DIII-D is to study the plasma response to variations in plasma control parameters for a variety of plasma confinement regimes. Typically a single plasma variable is chosen with the choice based upon a known and ideally strong response. Examples of such variables are plasma elongation (κ), safety factor (q), electron to ion temperature ratio T_e/T_i, gradients in T_e and T_i, etc. A strong plasma response facilitates these studies by providing clear changes for comparison and also by raising the results out of naturally occurring noise and fluctuation levels. Disagreements between measurements and simulations are significant as they can shed light on the underlying physics model limitations. Since conclusions based upon a single radial position or single parameter (e.g. $\tilde{n}/n$ only) can be misleading it is found to be highly important to compare a variety of measurement types and scales as well as radial profiles. Figure 2 uses data from a plasma elongation (κ) experiment conducted on DIII-D to illustrate this approach. Plasma elongation is a useful parameter due to its known strong effect on plasma confinement in tokamaks [26]. The figure shows turbulent electron temperature fluctuations over the frequency range 0–200 kHz for two plasma elongation shapes, $\kappa = 1.4$ and 1.1. The fluctuation levels are significantly larger for the low κ shape. In addition, it was found that the energy confinement is also lower for the lower κ shape. For this example, a simulation prediction that has high fidelity (defined here as the degree to which the simulation accurately reproduces experiment) will predict the variation of $\tilde{T}_e$ with κ and radius as well as the quantitative values. A lower fidelity simulation might predict the trends (e.g. the increase in $\tilde{T}_e$ with κ) but not the magnitudes. Note that in validation studies, comparisons are made with as large a range of measurements as possible (discussed further in the next section). In so doing, the study seeks to reveal aspects of the simulation code that require further investigation.

3. Tools available at DIII-D

The DIII-D tokamak has a significant number of profile and fluctuation diagnostics available for validation studies. Profile diagnostics include charge exchange recombination (CER) for T_i, impurity density, toroidal and poloidal rotation, and electric field profiles; motional Stark effect (MSE) for core safety factor profiles; Thomson scattering for T_e and n_e; ECE for T_e; and reflectometry for n_e profiles. Fluctuation diagnostics include beam emission spectroscopy (BES) for low-k $\tilde{n}_e$ and turbulence flows, Doppler backscattering (DBS) for turbulence flows and intermediate-k $\tilde{n}_e$, millimetre wave backscattering for high-k $\tilde{n}$, CECE for low-k electron temperature fluctuations $\tilde{T}_e$ and phase contrast imaging (PCI) for low-through-intermediate-k $\tilde{n}_e$. These diagnostics have differing operational requirements as well as differing wavenumber, spatial and temporal resolutions. The individual diagnostic requirements and limitations must be accounted for in the design of the experiment as well as in the design of the synthetic diagnostic used to interpret the simulation predictions. The available diagnostics are diagrammatically related to various instability wavenumbers of interest in figure 3. This figure shows wavenumber ranges and available measurements. For example, in the trapped electron mode (TEM) wavenumber range both PCI and DBS make measurements. Other overlapping measurements include BES and reflectometry for low-k $\tilde{n}$. As with multiple measures of equilibrium parameters (e.g. ECE and Thomson scattering for T_e) these provide checks and verifications of the fluctuation measurements. Recently added measurements include local, wavenumber resolved TEM scale $\tilde{n}$, fluctuating turbulence flows, and density–temperature (n_e–T_e) turbulence crossphase. The novel measurement of the n_e–T_e crossphase is important in gyrokinetic validation studies since it represents the relationship between different fluctuating fields—density and temperature (it is also closely related to the crossphase that determines the turbulent transport) and since it can be directly compared with simulation at a fundamental level. The unique array of multifield, multiscale turbulence measurements has been utilized to study a wide range of target plasmas with excellent spatial coverage (the typical radial range of these studies is $\rho \sim 0.55$–0.85 although a larger range is possible).

The DIII-D tokamak is a medium sized tokamak, with major radius $R \sim 1.7$ m, minor radius $a \sim 0.6$ m, magnetic field $B = 0.6$–2.1 T, plasma current 1–2 MA, elongation

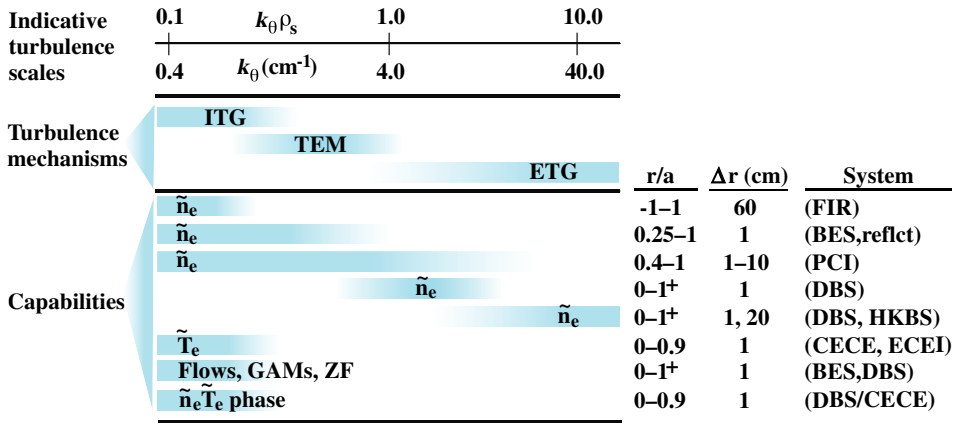

Figure 3. Multifield and multiscale fluctuation diagnostics on DIII-D. The figure compares the wavenumber ranges of representative instabilities with the diagnostic wavenumber range. Diagnostic system, measurement, approximate spatial coverage and spatial resolutions are also indicated.

Table 1. Parameters utilized and variation achieved in validation studies at DIII-D.

Parameter	Variation (%)	Plasma
T_e/T_i	30	L-mode (this paper)
Local L_{T_e}	50	L-mode [28]
$\tilde{n}_e$–$\tilde{T}_e$ crossphase	50	L-mode [29]
Elongation, κ	30	L-mode [26]
T_e/T_i	25	Hybrid H-mode
T_e/T_i	50	QH-mode [26, 32]

$\kappa \sim$ 1–2, ~20 MW neutral beam injection, ~3.4 MW electron cyclotron heating and $\leqslant$4.5 MW fast wave heating. Plasma shaping and control are very flexible with a large range in size, triangularity, elongation, etc possible. This parameter range, shaping flexibility, heating choices and broad diagnostic coverage combine to make DIII-D an excellent choice for validation studies.

Validation studies are focused on the testing and validation of a wide range of gyrokinetic turbulence codes/simulations. The simulation code most extensively utilized to date for validation studies at DIII-D is GYRO [18, 19] and more recently GEM [20], GENE [21], GS2 [22], GTC [27] and GYSELA [28] have begun to enter the process. GYRO is a physically comprehensive non-linear gyrokinetic code containing multiple gyrokinetic ion species, trapped and passing electrons (drift or gyrokinetic), electron and ion pitch angle collisions, electromagnetic effects, $E \times B$ and parallel flow shears, real geometry, $E \times B$ and magnetic flutter transport. GYRO can be run in either a local flux tube or a global simulation mode. Here flux tube generally means that the gradients of interest (L_n, L_{T_i}, etc) do not vary across the simulation domain whereas in a global simulation they are allowed to vary.

4. Experiments performed

A series of plasma experiments were performed for validation studies at DIII-D. The target plasmas were selected to address plasma parameters that have a large plasma response such that both experiment and simulation show significant variations. Table 1 illustrates the range of plasma parameters addressed, percentage parameter variation achieved, and the plasma confinement regime utilized. Note that the largest variations achieved are of order 50% with some as small as 25%. Planned future studies include scans of safety factor q and collisionality. In the next section the results from the L-mode T_e/T_i scan experiment shown in table 1 are examined in detail and compared with simulation.

5. L-mode T_e/T_i scan experimental measurements and comparison with simulation

5.1. Plasma description

The effect of varying T_e/T_i in an L-mode, diverted plasma was examined by applying ECH heating to an NBI heated plasma. The base case was a sawtooth-free upper single null plasma, chord-averaged electron density $n_{avg} = 2 \times 10^{19}$ m^{-3}, toroidal magnetic field $B_T = 2.05$ T, plasma current $I_p = 1$ MA, neutral beam power $P_{NBI} = 2.5$ MW and safety factor at the 95% flux surface $q_{95} \approx 5.1$. T_e was increased via approximately 3.3 MW of electron cyclotron heating applied near radial location $\rho = 0.2$. The experimental goal was to keep the other plasma parameters of interest as similar as possible, with the exception of the desired change in T_e/T_i, between the two cases. Figure 4 shows profiles of interest for the two cases, lower T_e (heated by Ohmic and NBI only, here termed the low T_e/T_i case) and higher T_e (Ohmic, NBI and ECH, here termed the high T_e/T_i case). An increase is observed in the electron temperature with some variation in the other parameters as well. The radial range of interest for these validation studies is $\rho = 0.5$–0.8. In this range the ratio T_e/T_i is seen to increase by ~30% in the radial range $\rho = 0.5$–0.8, with the largest variation in other parameters occurring in the inverse ion temperature scale length a/L_{T_i} and collisionality. Changes in these parameters affect the stability calculations for the various instabilities of interest (e.g. ion temperature gradient (ITG), TEM, ETG instabilities) and must be accounted for. Although it is preferred and simpler if only one parameter is varied, the plasma simulations will take into account all measured changes allowing a consistent

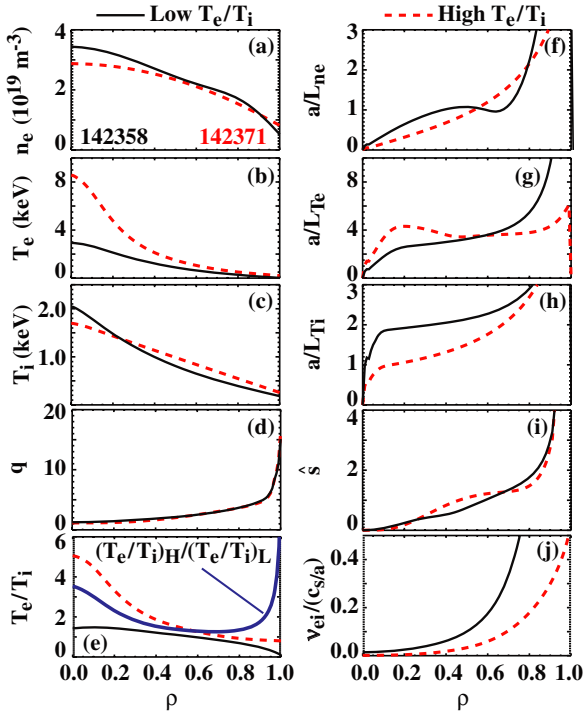

Figure 4. Radial profiles of measured (*a*) n_e, (*b*) T_e, (*c*) T_i, (*d*) q, (*e*) T_e/T_i ratio, normalized inverse scale lengths, (*f*) a/L_{n_e}, (*g*) a/L_{T_e}, (*h*) a/L_{T_i}, (*i*) magnetic shear $s = \mathrm{d}\ln q/\mathrm{d}\ln r$ and (*j*) collisionality, ν_{ei}/C_s. Here a is the minor radius on the midplane, and c_s is the ion sound velocity. Low and high T_e/T_i cases corresponding to NBI only and NBI + ECH cases are shown. Note that (*e*) also shows the ratio of the T_e/T_i parameter for the two cases, denoted H for high T_e/T_i and L for low T_e/T_i.

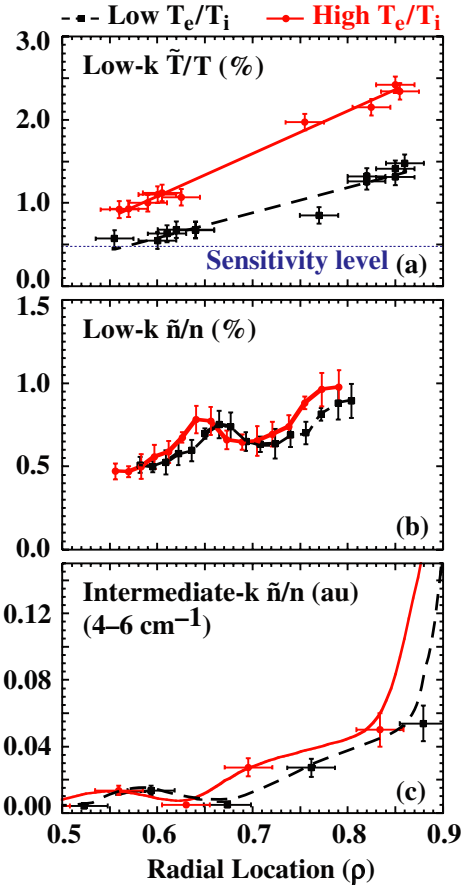

Figure 5. Experimental measurements: radial profiles of (*a*) low-k $\tilde{T}_e$ (CECE), (*b*) low-k $\tilde{n}$ (BES) and (*c*) intermediate-k $\tilde{n}$ (DBS) for low and high T_e/T_i cases. Solid lines are guides for the eye.

comparison. The decrease in a/L_{T_i} with ECH will generally result in lower ITG mode growth rates while the decrease in collisionality with ECH will result in higher TEM growth rates. The situation in the plasma, where the various instabilities are coupled via the background plasma, can be more complicated.

5.2. Fluctuation measurements

Radial profiles of multiple fluctuation fields and wavenumbers were obtained for the low and high T_e/T_i cases. Profiles of low-k electron temperature fluctuation levels ($\tilde{T}_e/T_e$ from CECE) covering the radial range $\rho = 0.5$–0.8 are shown in figure 5(*a*). The normalized fluctuation levels are typical of the core of L-mode plasmas, being in the range 0.5% to 3%. The $\tilde{T}_e/T_e$ fluctuation levels increase by as much as 70% comparing the high with the low case. In contrast, the low-k density fluctuations ($k < 3\,\mathrm{cm}^{-1}$, from BES) showed only small changes comparing the low and high T_e/T_i cases (figure 5(*b*)). Radial profiles of intermediate-k density fluctuations (from DBS) show no discernable change (figure 5(*c*)). Examination of wavenumber spectra of these intermediate-k $\tilde{n}$ ($k \sim 3.5$–$6\,\mathrm{cm}^{-1}$, from DBS) at $\rho = 0.55$ (not shown) showed some signs of redistribution of power in k space; however, the levels remain roughly unchanged. High-k density fluctuations ($k \sim 3.5\,\mathrm{cm}^{-1}$) from millimetre wave backscattering (not shown) indicate little change as well. Thus the strongest response was in the low-k temperature fluctuations $\tilde{T}_e/T_e$ with a smaller change in the low-k density fluctuations $\tilde{n}/n$.

5.3. Linear gyrofluid growth rate predictions

The trapped-gyro-Landau-fluid (TGLF) code [29] was used to examine the linear growth rates $\rho = 0.6$ for the two plasma conditions shown in figure 6. The TGLF code solves the TGLF equations, and provides a fast and accurate approximation to the linear eigenmodes of drift-wave type instabilities (trapped ion and electron modes, ITG and ETG modes, and kinetic ballooning modes). It has been benchmarked and tested against the linear gyrokinetic code GKS [30]. The code calculates linear growth rates and frequencies for toroidal driftwaves corresponding to poloidal wavenumbers. Code inputs were the measured T_e, T_i, n_e, impurity profiles (assuming that fully stripped carbon is the major impurity) and magnetic equilibrium (the profiles used are shown in figure 4). The effects due to up–down plasma asymmetries or $E \times B$ velocity shear flow (E and B are local electric and magnetic fields) are not included in TGLF linear stability calculations. Linear calculations do not simulate the fully developed turbulence but they can provide a guide as to where particular instabilities

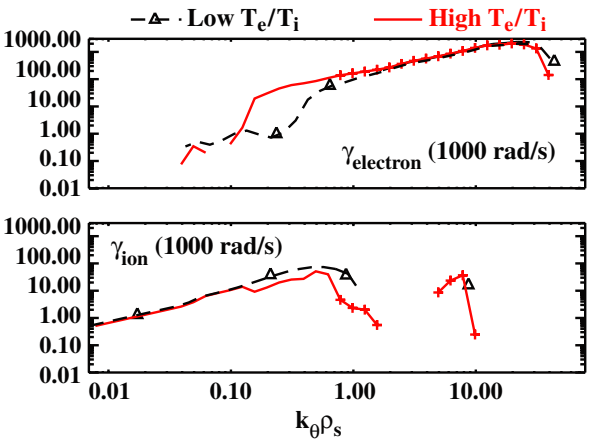

Figure 6. Linear growth rates for radial location $\rho = 0.6$ from the TGLF code for ion and electron modes versus wavenumber for low and high T_e/T_i cases.

might be unstable and how they might behave with given changes in the underlying plasma parameters.

Figure 6 shows the linear growth rates corresponding to ion and electron modes for the two plasma cases, low and high T_e/T_i. Here an ion (or electron) mode is designated as such based upon the sign of the real frequency as calculated in TGLF. Negative frequencies correspond to propagation in the ion diamagnetic direction while positive is in the electron diamagnetic direction. These are designated as ion and electron modes respectively. Ion mode growth rates in the low k_θ range $k_\theta\rho_s = 0.1$–1.0 decrease with the additional ECH, while electron mode growth rates increase in this same low k_θ range. Higher k_θ ($k_\theta > 10\,\mathrm{cm}^{-1}$) ion modes are calculated to be stable in both plasmas. Little change is observed for the higher k_θ electron type modes with the additional ECH. If electron mode growth rates are associated with electron temperature fluctuations and intermediate to high k_θ density fluctuations (TEM and ETG instabilities) and ion mode growth rates with low-k_θ density fluctuations (ITG instabilities) then these calculations show some rough correspondence to the fluctuation measurements described above. Interestingly, the ion modes near $k_\theta\rho_s = 5$–10 in figure 6(*b*) have been identified as subdominant (in terms of growth rate), TEMs with a negative mode averaged curvature drift which gives rise to the propagation in the ion diamagnetic drift direction. It should be emphasized that the linear growth rates are only a very rough indication of how the plasma might respond and will not reflect any non-linear couplings and back reaction on the plasma, effects that should be contained in the fully non-linear simulations.

5.4. Non-linear gyrokinetic predictions

The non-linear GYRO code [18] was used to examine the fluctuations and transport at $\rho = 0.6$ for the two plasma conditions shown in figure 4. Flux-tube simulations were performed resolving wavenumbers $k_\theta\rho_s \leqslant 1.1$, where $\rho_s = 0.21\,\mathrm{cm}$ and $0.25\,\mathrm{cm}$ for the low and high T_e/T_i cases, respectively (ρ_s is the ion gyroradius evaluated using the local electron temperature). These simulations used the same input

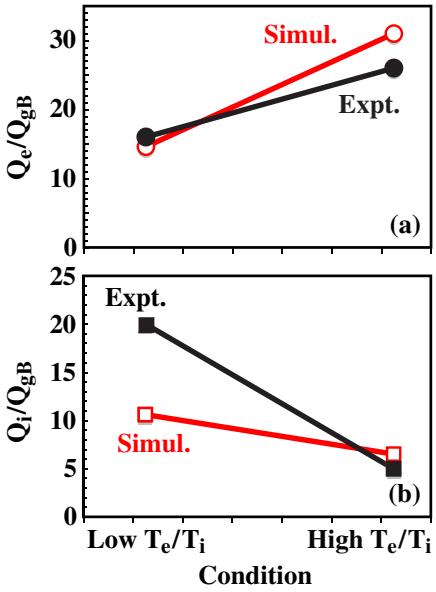

Figure 7. Simulation and experiment (*a*) electron and (*b*) ion thermal fluxes at $\rho = 0.6$ normalized to gyro-Bohm flux, $Q_{gB} = n_e c_s T_e$ for low and high T_e/T_i cases.

profiles (i.e. figure 4) as used in the TGLF calculations of section 5.3. Included in the simulations were the measured $E \times B$ shear as well as a single impurity species (carbon). The runs were electromagnetic, with mass ratio $(M_i/m_e)^{1/2} = 40$, where m_e is the electron mass and M_i is the main ion (deuterium) mass. Electrons are drift kinetic so that the effect of finite electron Larmor radius was excluded. Simulation grid parameters for the low T_e/T_i case are radial box size $L_x = 177\rho_s$, radial resolution $\Delta x/\rho_s = 0.67$ and 20 toroidal modes spanning $0 \leqslant k_\theta\rho_s \leqslant 1.07$. Similarly for the high T_e/T_i case the radial box size is $L_x = 141\rho_s$, radial resolution $\Delta x/\rho_s = 0.39$ and 20 toroidal modes spanning $0 \leqslant k_\theta\rho_s \leqslant 1.36$. Higher k non-linear simulations have not yet been performed; however, the indication from these lower k simulations is that the modes above $k_\theta\rho_s \approx 1$ (i.e. the higher k ETG scale modes in linear calculation shown in figure 6(*a*)) do not contribute significantly to the fluctuation level or transport for this radial location.

Figure 7 shows a comparison of the ion and electron thermal fluxes normalized with the gyro-Bohm flux, $Q_{gB} = n_e c_s T_e(\rho_s/a)^2$, at $\rho = 0.6$ from experiment and simulation. The normalization by $Q_{gB} \sim T_e^{5/2}$ obscures the amount of increase in absolute Q_e in the high T_e/T_i case (also note that absolute simulation Q_i increases in the high T_e/T_i case, whereas the normalized quantity decreases due to the $Q_{gB} \sim T_e^{5/2}$ variation). The fluxes are plotted versus the nominal plasma condition and show similar qualitative behaviour between the experimental and predicted values. The quantitative values for the electron fluxes also compare favourably. In contrast the quantitative ion fluxes for the low T_e/T_i case differ by a factor of two between simulation and prediction while being similar for the high T_e/T_i case. Note that these simulations use the profiles shown in figure 4 with no attempt at thermal flux matching or profile variation. These flux matching and variation studies are underway and some

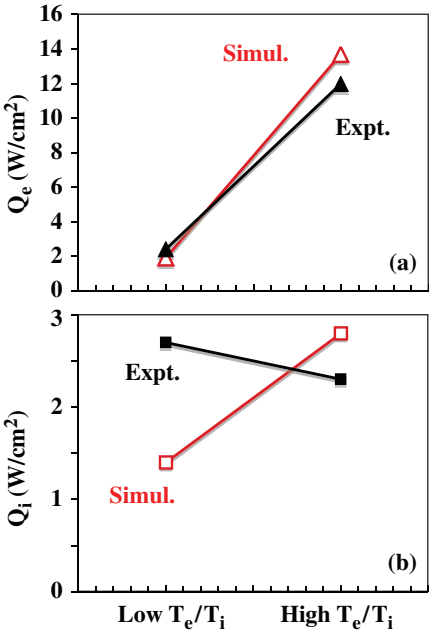

Figure 8. Simulation and experiment (*a*) electron and (*b*) ion thermal fluxes at $\rho = 0.6$ in physical units for low and high T_e/T_i cases.

improvement in the agreement may occur. Figure 8 shows the ion and electron thermal fluxes using physical units. The basic conclusions remain the same as with figure 7 with the exception that the trend of the simulated ion thermal flux with T_e/T_i is now inconsistent with the experimental values. This highlights the need for care when using normalized values since the conclusion from figure 7(*b*) is that the simulation correctly predicts the overall trend whereas figure 8(*b*) indicates both trend and magnitude disagree.

Figure 9 shows measured and GYRO predicted power and crossphase spectra for the low and high T_e/T_i cases. In all cases synthetic diagnostics [23–25] were used to analyse the simulation results for accurate comparison with the measurement. The predicted density fluctuation spectra are quite similar to measurement in both shape and magnitude, with the RMS $\tilde{n}$ levels being 0.41% predicted and 0.5% measured for the low T_e/T_i case (0.47% predicted and 0.55% measured for the high T_e/T_i case). The electron temperature fluctuation levels $\tilde{T}_e/T_e$ are overpredicted by GYRO being 0.86% predicted and 0.62% measured for the low T_e/T_i case (2.2% predicted and 1.1% measured for the high T_e/T_i case). Note, however, that the simulation does predict an increase in $\tilde{T}_e/T_e$ for the high T_e/T_i case in qualitative agreement with measurement. The density–temperature crossphase spectra are shown in figures 9(*c*) and (*f*). Here the agreement between experiment and simulation is quite good in both magnitude and change with T_e/T_i. Table 2 summarizes the measured and predicted values for the two cases. For these cases the effect of profile uncertainties on the model predictions has not yet been evaluated and so no uncertainties or error bars are indicated in table 2. Future work will focus on these effects.

Non-linear GYRO simulations were attempted for radial location $\rho = 0.8$. However, physically meaningful solutions have not been obtained to date at this location, with the simulations exhibiting an unphysical accumulation of fluctuation energy at the highest simulation wavenumbers ($k_\theta \rho_s \sim 1$ to 1.5). This phenomenon is known to correlate with strong intermediate to high-k growth rates, suggesting a need for multiscale simulations (e.g. coupled ITG–TEM–ETG) and is currently under further investigation. The radial location where this effect begins to manifest itself is also of importance and studies are underway to determine this as well.

5.5. Transport model simulations

In addition to the just described non-linear GYRO simulations, transport model simulations using the TGLF theory-based transport model (the TGLF code) were also performed for the low and high T_e/T_i cases. These simulations were run using a transport solution or flux matching methodology (as implemented in the TGYRO code [16]). This methodology utilizes the fast TGLF code to calculate quasi-linear fluxes based on a starting set of density and temperature profiles. The modelled fluxes are then compared with the measured fluxes. The profiles are next modified in an iterative manner with the thermal fluxes recalculated at each step until a match of the modelled fluxes with the measured fluxes is obtained. Along the way the inputs are self-consistently modified, i.e. as T_e is changed so are the resulting T_e/T_i ratio, collisionality, ion–electron energy exchange term, etc resulting in self-consistent changes to the local growth rates, phase angles, quasi-linear fluxes, etc. The results of this modelling are shown in figures 10 and 11. The thermal fluxes (figures 10(*a*), (*c*) and 11(*a*), (*c*)) are seen to be well matched out to radii of $r/a \sim 0.85$. The resulting temperature profiles are generally within the profile uncertainty with the exception of the very central T_e in the high T_e/T_i case (figure 11(*b*)). It is possible that a better T_e match in the core region of this high T_e/T_i case could be obtained with further simulations varying, for example, local density gradients. Note that the flux matching was not obtained for radii $r/a \sim 0.85$ in either the low or high T_e/T_i cases (figures 10 and 11) being significantly under predicted in both cases. Physically, this underprediction arises because the experimentally measured parameters (gradients, collisionality, etc) do not produce sufficient model calculated flux to match the experiment. In order to increase and therefore match the flux, the model calls for a larger local gradient. In the case of figures 10 and 11, the required gradient change is larger than physically possible (i.e. it requires the temperature to become negative) so that the model defaults the temperature to the base or unperturbed value. A similar underprediction was reported by Holland *et al* [23] for a different L-mode condition and there it was also associated with an underprediction of the fluctuation levels.

These observations fit a general trend for L-mode validation studies at DIIID in that predictions of transport and fluctuation levels in the mid-core region ($0.4 < \rho < 0.75$) are often in better agreement with experiment than those in the outer region ($\rho > 0.75$) [23, 24, 31, 33, 34]. As a further illustration, figure 12 shows experimental profiles and simulations from DIII-D shot 128913, an L-mode shot used extensively in validation studies [23–25, 34]. This shot is an upper single-null plasma, with $B_z = 2.1\,\mathrm{T}$, $I_p = 1\,\mathrm{MA}$,

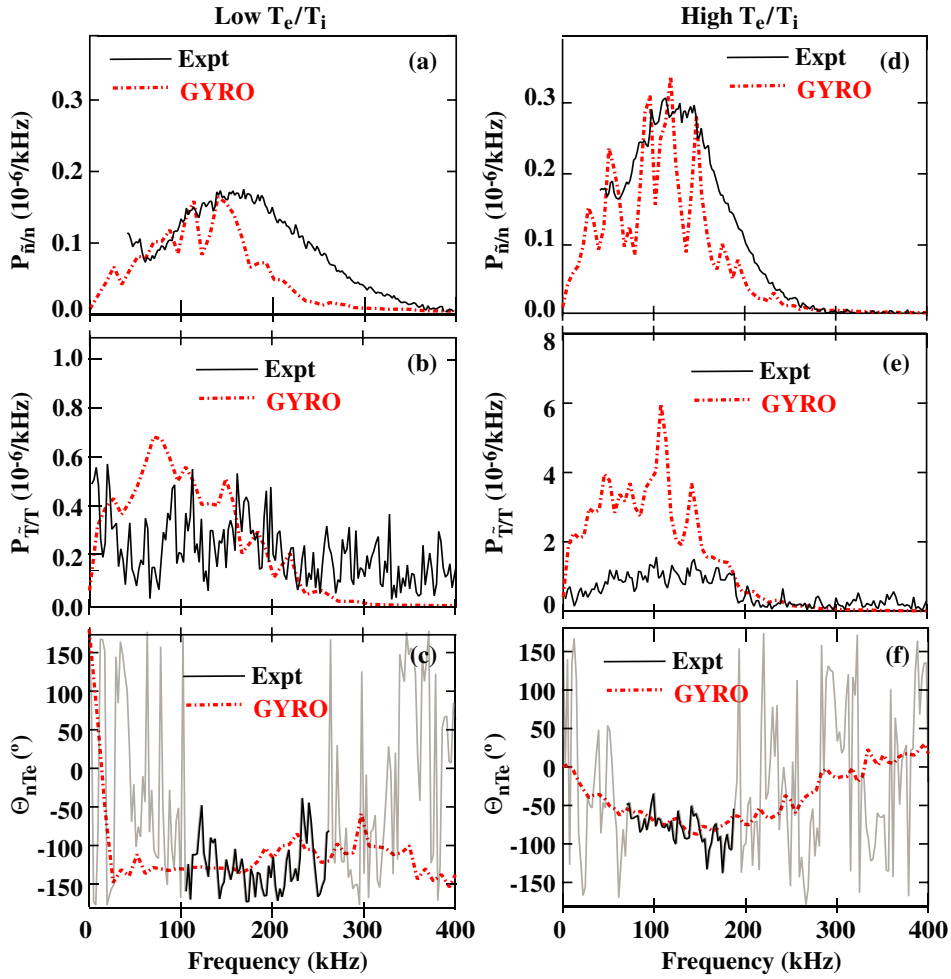

Figure 9. Measured and GYRO simulated power spectra at radial location $\rho = 0.6$ for electron density fluctuation levels $(\tilde{n}/n)^2$) (*a*), (*d*), electron temperature fluctuation levels $(\tilde{T}_e/T_e)^2$ (*b*), (*e*), and electron density–temperature fluctuation cross phase Θ_{nT} (*c*), (*f*). Left and right hand columns are low and high T_e/T_i cases, respectively.

Table 2. Measured and GYRO predicted fluctuation and transport values for low and high T_e/T_i cases at radial location $\rho = 0.6$.

	Low T_e/T_i		High T_e/T_i	
Parameter	Experiment	GYRO	Experiment	GYRO
$\tilde{T}_e/T_e$	0.62%	0.86%	1.1%	2.2%
$\tilde{n}/n$	0.41%	0.50%	0.47%	0.55%
n_e–T_e crossphase, Θ_{nT}	−131°	−125°	−77°	−70°
Q_e	2.4 W cm^{-2}	1.9 W cm^{-2}	12 W cm^{-2}	13.7 W cm^{-2}
Q_i	2.7 W cm^{-2}	1.4 W cm^{-2}	2.3 W cm^{-2}	2.8 W cm^{-2}

$q_{95} = 5.1$, chord-averaged density $\langle n_e \rangle = 2.3 \times 10^{23}$ cm^{-3} and ∼2.5 MW co-injected neutral beam power. The inputs to GYRO and TGLF codes are the measured profiles, i.e. figure 12(*a*) and magnetic equilibrium. For these simulations the GYRO parameters are approximately radial box size $L_x = 110$–$120\rho_s$, resolution $\Delta x/\rho_s = 0.4$–0.5 (here x is the radial coordinate) and 16 toroidal modes spanning $0 \leqslant k_\theta \rho_s < 1$ [35]. The error bars in the TGLF predictions were derived using the standard deviation of 1728 TGLF runs with input profiles (n_e, T_e, T_i) randomly varied within experimental uncertainties. The statistical uncertainty in the GYRO predictions were derived using the standard deviation of the mean fluxes obtained from the simulation time histories (with the means themselves from averages over time periods longer than the turbulence autocorrelation times). The integrated energy flows through the local surface area (P_e and P_i) from both transport modelling using TGLF and non-linear GYRO show qualitative and some quantitative similarity to experiment in the radial range $\rho < 0.6$. However, as ρ increases, significant underprediction of the fluxes (figures 12(*b*) and (*c*)) begins near $\rho \sim 0.65$ and approaches a 50% or larger underprediction near $\rho = 0.7$ and beyond.

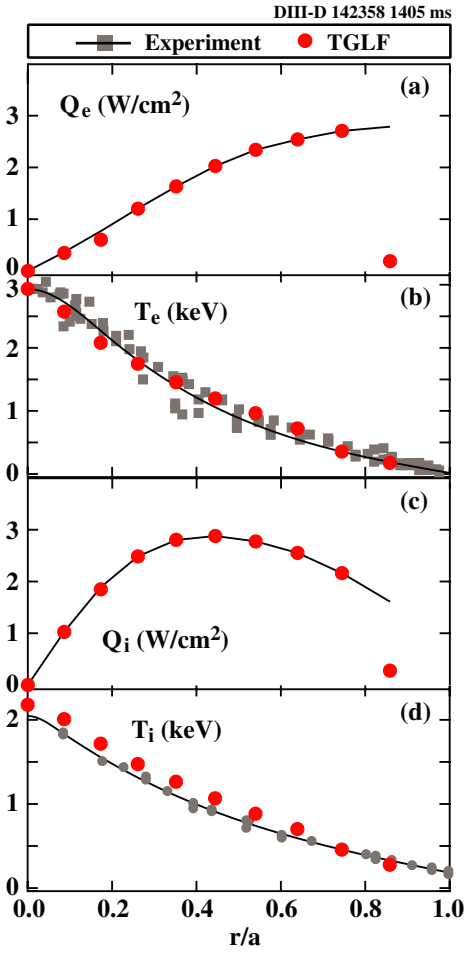

Figure 10. TGYRO/TGLF model transport matched (also termed flux matched) solutions for low T_e/T_i case. (*a*), (*c*) are electron and ion thermal fluxes, experiment is a solid line, model is filled circles, (*b*), (*d*) are comparisons of measured (squares) and predicted (circles) electron and ion temperature profiles.

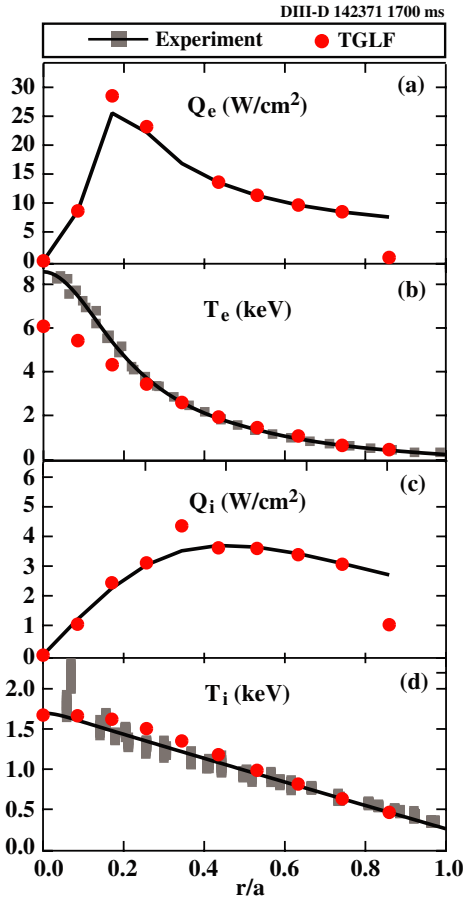

Figure 11. Flux matched transport solutions using the TGYRO/TGLF model for high T_e/T_i case. (*a*), (*c*) are electron and ion thermal fluxes, experiment is a solid line, model is filled circles, (*b*), (*d*) are comparisons of measured (squares) and predicted (circles) electron and ion temperature profiles.

These flows are based on the experimental profiles shown in figure 12(*a*). Improved simulation-experiment matching has been obtained in the core of this discharge using a flux matching or transport solution [16]. As discussed earlier this method allows the input profiles to change in order to match the ion and electron thermal fluxes. Note, however, that even with flux matching the radii towards the edge were underpredicted [16] similar to what is seen in figures 12(*b*) and (*c*). Recent simulations using the GEM code are also shown in figure 12. GEM is an electromagnetic, gyrokinetic delta-f particle-in-cell turbulence simulation with realistic equilibrium profiles and geometry [20]. For these calculations GEM used a radial box size of approximately 62.4 ρ_i (ρ_i is the ion gyroradius), with the resolved wavenumbers k_θ being $0.1 \leqslant k_\theta \rho_i \leqslant 0.8$. A grid of 64 (toroidal direction) $\times$ 64 (radial direction) $\times$ 32 (along the field line) with perpendicular cell size of $\sim 0.98\rho_i$ was used. There were 128 ions and 128 electrons per grid cell. The GEM predictions of P_e and P_i are comparable to experiment at $\rho = 0.5$ while significantly underpredicting experiment at $\rho = 0.75$. The GEM results are seen to be very consistent with the GYRO and TGLF predictions and are significant as they indicate that the underprediction towards the edge is not a code specific issue.

6. Summary and conclusions

Validation studies on DIII-D are focused on the testing of a range of gyrokinetic turbulence codes/simulations. Through this ongoing validation activity, where experimental measurement is compared in detail with simulation prediction, the design of suitably rigorous experiments for testing code predictions has steadily improved. Comparison of L-mode low and high T_e/T_i cases finds that GYRO non-linear simulations of electron density fluctuation levels $\tilde{n}/n$ and electron thermal transport Q_e are comparable to measured levels at $\rho = 0.6$. Furthermore, the observed changes in these parameters for the two cases, low and high T_e/T_i, are reasonably well predicted by simulation. Quite surprising is the excellent agreement between predicted and measured electron density–temperature fluctuation crossphase and the changes associated with the two T_e/T_i cases. On the other hand, simulation significantly overpredicts the electron temperature fluctuation

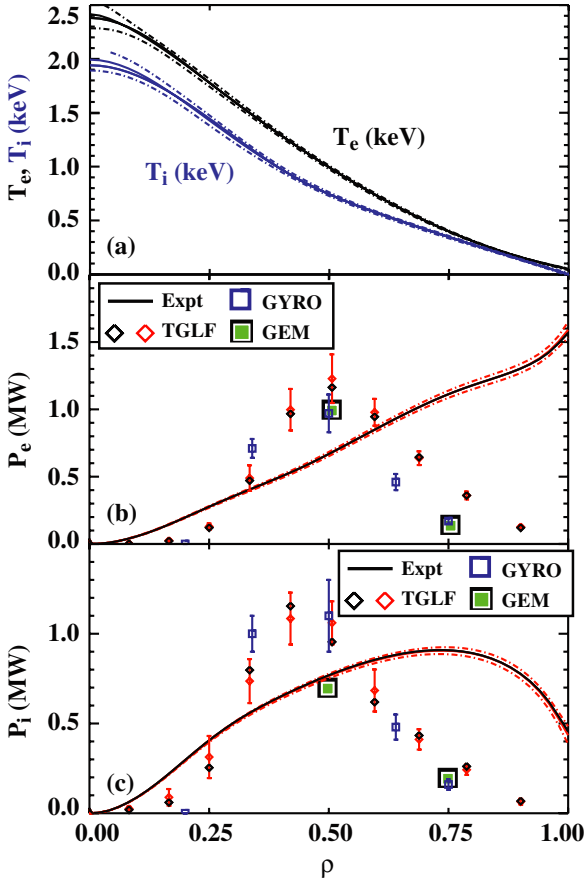

Figure 12. (*a*) Experimental T_e, T_i, (*b*) experimental and predicted electron energy flow through the local surface area (P_e), (*c*) experimental and predicted ion energy flow through the local surface area (P_i).

$\tilde{T}_e/T_e$ level by as much as a factor of two. The general increase in $\tilde{T}_e/T_e$ in going from the low to the high T_e/T_i case is, however, reproduced by simulation. Neither the magnitude of the ion thermal flux Q_i nor its variation with T_e/T_i is well predicted by the simulation. Improvement in the experiment–simulation matching may be possible by varying the various scale lengths, temperatures, densities, etc within their respective uncertainties; however, this has not yet been performed. Several conclusions can be drawn from this work. The observation that the fundamental level quantity, the n–T crossphase, is well predicted by simulation along with matching of some higher level quantities ($\tilde{n}/n$, Q_e) may indicate that the simulation fairly adequately captures the essential physics at this radial location ($\rho = 0.6$). The simulation predictions of $\tilde{T}_e/T_e$ and Q_i could conceivably be better matched given sufficient computational effort (e.g. by varying the scale lengths within the uncertainties or by applying a flux matched solution methodology). On the other hand the underprediction of transport (and fluctuation levels [23]) as the L-mode edge is approached ($\rho \gtrsim 0.75$ or so) for multiple plasmas almost certainly indicates missing or incorrect physics within the gyrokinetic codes. Some partial resolution of this discrepancy might be obtained with highly computationally intensive coupled low-through-high-k simulations (e.g. [36, 37]). In addition, effects such as turbulence spreading/coupling [11] or avalanche type effects [12] may be important in this region. More work in this important region is certainly called for. For example, although the simulation–measurement matching of higher level quantities (e.g. transport fluxes, fluctuation levels) towards the edge is poor, a comparison of fundamental level quantities such as the n–T crossphase (or correlation lengths, etc) may shed light on the underlying physics. This is currently not possible due to lack of converged non-linear solutions at larger radii in plasmas where the n–T crossphase measurement has been made (e.g. this paper and [29]). Work is underway to obtain non-linear solutions in these regions.

Acknowledgments

This work was supported by the US Department of Energy under DE-FG02-08ER54984, DE-FC02-04ER54698, DE-FG02-95ER54309, DE-FC02-93ER54186, DE-FG02-07ER54917, DE-FG02-89ER54296, DE-FG02-08ER54999 and DE-AC02-09CH11466. The research was performed in collaboration with the Center for Simulations of Plasma Microturbulence, and used resources of the National Center for Computational Sciences at Oak Ridge National Laboratory, which is supported by the Office of Science of the Department of Energy under Contract DE-AC05-00OR22725.

References

[1] Dawson J.M. *et al* 1991 *Int. J. High Perform. Comput. Appl.* **5** 13
[2] Tang W.M. 2002 *Phys. Plasmas* **9** 1856
[3] Mikkelsen D.R. *et al* 2002 *Proc. 19th IAEA Fusion Energy Conf. (Lyon, France, 14–19 Oct.)* (Vienna: IAEA) CD-ROM file EX/P5-03 and http://www.iaea.org/programmes/ripc/physics/fec2002/html/fec2002.htm
[4] Ernst D.R. *et al* 2004 *Phys. Plasmas* **11** 2637
[5] Horton W., Hoang G.T., Bourdelle C., Garbet X., Ottaviani M. and Colas L. 2004 *Phys. Plasmas* **11** 2600
[6] Angioni C. *et al* 2005 *Phys. Plasmas* **12** 040701
[7] Mantica P., Thyagaraja A., Weiland J., Hogeweij G.M.D. and Knight P.J. 2005 *Phys. Rev. Lett.* **95** 185002
[8] Peeters A.G. *et al* 2005 *Nucl. Fusion* **45** 1140–7
[9] Lin L. *et al* 2009 *Phys. Plasmas* **16** 012502
[10] Casati A. *et al* 2009 *Phys. Rev. Lett.* **102** 165005
[11] Lin Z. and Hahm T.S. 2004 *Phys. Plasmas* **11** 1099
[12] Diamond P.H. *et al* 2001 *Nucl. Fusion* **41** 1067
[13] Roache P.J. 1998 *Verification and Validation in Computational Science and Engineering* (Albuquerque, NM: Hermosa Publishers)
[14] Oberkampf W.L. and Trucano T.G. 2008 *Nucl. Eng. Des.* **238** 716–43
[15] Terry P.W. *et al* 2008 *Phys. Plasmas* **15** 062503
[16] Candy J., Holland C., Waltz R.E., Fahey M.R. and Belli E. 2009 *Phys. Plasmas* **16** 060704
[17] Barnes M. *et al* 2010 *Phys. Plasmas* **17** 056109
[18] Candy J. and Waltz R.E. 2003 *J. Comput. Phys.* **186** 545
[19] Candy J. and Waltz R.E. 2003 *Phys. Rev. Lett.* **91** 045001
[20] Chen Y. and Parker S.E. 2007 *J. Comput. Phys.* **220** 839
[21] Jenko F., Dorland W. and Hammett G.W. 2001 *Phys. Plasmas* **8** 4096
[22] Dorland W., Jenko F., Kotschenreuther M. and Rogers B.N. 2000 *Phys. Rev. Lett.* **85** 5579
[23] Holland C. *et al* 2009 *Phys. Plasmas* **16** 052301
[24] White A.E. *et al* 2008 *Phys. Plasmas* **15** 056116

[25] White A.E. *et al* 2008 *Rev. Sci. Instrum.* **79** 103505
[26] Petty C.C. 2008 *Phys. Plasmas* **15** 080501
[27] Lin Z. *et al* 1998 *Science* **281** 1835
[28] Grandgirard V. *et al* 2007 *Plasma Phys. Control. Fusion* **49** B173
[29] Staebler G.M., Kinsey J.E. and Waltz R.E. 2005 *Phys. Plasmas* **12** 102508
[30] Kotschenreuther M., Rewoldt G.W. and Tang W.M. 1995 *Comput. Phys. Commun.* **88** 128
[31] Holland C. *et al* 2011 Advances in validating gyrokinetic turbulence models against L and H-mode plasmas *Phys. Plasmas* at press
[32] Schmitz L. *et al* 2010 Reduced electron thermal transport in low collisionality H-mode plasmas in DIII-D and the importance of intermediate/small-scale turbulence *23rd IAEA Fusion Energy Conf. (Daejon, Korea, 11–16 Oct.)* EXC/P7-01 http://www-pub.iaea.org/mtcd/meetings/cn180_papers.asp
[33] DeBoo J.C. *et al* 2010 *Phys. Plasmas* **17** 056105
[34] White A.E. *et al* 2010 *Phys. Plasmas* **17** 056103
[35] Holland C. *et al* 2008 *J. Phys. Conf. Ser.* **125** 012043
[36] Waltz R.E., Candy J. and Fahey M. 2007 *Phys. Plasmas* **14** 056116
[37] Görler T. and Jenko F. 2008 *Phys. Plasmas* **15** 102508